Pure Appl. Chem., Vol. 81, No. 8, pp. 1449–1457, 2009.
doi:10.1351/PAC-CON-08-11-06

Aerosol-generated mesoporous silicon oxycarbide particles*

Alberto Pauletti‡, Guillaume Moskowitz, Thomas Millan, Cristina Fernández-Martín, Cédric Boissière, Christel Gervais, and Florence Babonneau

Laboratoire de Chimie de la Matière Condensée de Paris, Université Pierre et Marie Curie-Paris 6 and CNRS UMR 7574, Collège de France,11 Place M. Berthelot, 75231 Paris Cedex 05, France

Abstract: Aerosol-generated mesoporous organosilica submicronic spheres have been converted into porous silicon oxycarbide (SiCO) glasses by pyrolysis at 1000 °C in an inert atmosphere. Spherical mesoporous particles obtained from acidic solutions of 1,2-bis(triethoxysilyl)ethane and Pluronic® F127 structuring agent were characterized by X-ray diffraction (XRD), transmission electron microscopy (TEM), N_2 adsorption/desorption, and multinuclear solid-state magic-angle spinning (MAS) NMR. These particles were then pyrolyzed at 1000 °C and transformed into a SiCO phase as evidenced by ^{29}Si MAS NMR, while TEM shows preserved mesoporosity, unfortunately difficult to access owing to the presence of an outer layer of dense silica.

Keywords: silicon oxycarbide; nanoparticles; porosity; aerosol; template.

INTRODUCTION

After the discovery of ordered mesoporous silica in 1992 synthesized in solution via the self-assembly of inorganic precursors and amphiphilic molecules [1], three research groups independently synthesized in 1999 a new class of mesoporous materials designated as periodic mesoporous organosilicas (PMOs) [2–4]. PMOs are prepared with bridged organotrialkoxysilane precursors $(RO)_3Si–X–Si(OR)_3$ instead of tetraalkoxysilane so that organic groups X are part of the silica matrix walls (Fig. 1).

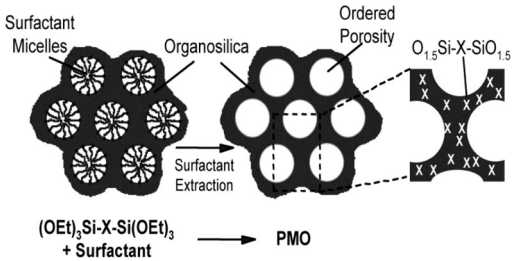

Fig. 1 Schematic representation of the synthetic route to PMOs.

*Paper based on a presentation at the 8th Conference on Solid State Chemistry, 6–11 July 2008, Bratislava, Slovakia. Other presentations are published in this issue, pp. 1345–1534.

‡Corresponding author

The first PMO powders were synthesized from short alkyl chain bridges in the presence of cationic surfactants as structure-directing agents in basic media. Further studies focused on the enlargement of the pore diameter by using non-ionic triblock copolymers as structure-directing agents. The most common ones are the triblock Pluronic® P123 ($EO_{20}PO_{70}EO_{20}$) and Pluronic F127 ($EO_{106}PO_{70}EO_{106}$). Bifunctional PMOs have also been synthesized by either co-condensation of bridged bis(trialkoxysilyl)organosilanes and terminal (trialkoxysilyl)organosilanes or co-condensation of two different bissilylated precursors in the presence of a structure-directing agent. For a more complete overview of the field of PMOs, see the reviews from Fröba et al. [5,6]. Recently, it was shown that PMOs can be used to produce porous silicon oxycarbide (SiCO) glasses [7–10]. The principle is based on self-assembly of silylated precursors $(RO)_3Si–X–Si(OR)_3$ and surfactants used as amphiphilic templating agents. The obtained hybrid materials that contain both Si–C and Si–O bonds and periodic mesoporosity after removal of the templating agent are suitable precursors for porous SiCO glasses in which carbon atoms are introduced in a silica network through mixed SiC_xO_{4-x} tetrahedra. The presence of covalent Si–C bonds imparts better chemical, mechanical, and thermal properties compared to pure silica [11,12]. Moreover, the presence of mesoporosity offers scope for applications in the field of catalysis or separation techniques [13,14], especially if harsh experimental conditions, for example, in terms of temperature are required.

Up to now, these PMOs have essentially been prepared via powder precipitation. Cubic and hexagonal structures have been obtained starting from bis-silylated precursors and ionic surfactants like cetyltrimethylammoniumchloride [7,8] but after pyrolysis, only the cubic phase retained porosity up to 1273 K and displayed a true SiCO phase. Using Pluronic F127 and P123 triblock copolymers as surfactants, cubic and hexagonal phases were obtained, respectively, and a porous SiCO was only obtained in the first case [9,10].

A new approach known as evaporation-induced self-assembly (EISA) [15] can also be considered to generate particles with controlled spherical morphology. This process is based on the progressive concentration of nonvolatile species during solvent evaporation. Self-assembly thus occurs in liquid films or inside droplets, leading to the formation of mesostructured films, membranes, or particles. This process has been extensively used to produce mesoporous thin films [16], and has also been extended to produce spherical submicronic particles using an aerosol technique [17]. Mesoporous silica [18,19] as well as titania [20] particles have been produced. In this study, we have therefore investigated the possibility to generate PMO powders by spray drying and to convert the resulting spherical particles into porous SiCO glasses.

EXPERIMENTAL PROCEDURE

Synthesis

1,2-Bis(triethoxysilyl)ethane (BTEE 97 %, provided by Gelest), non-ionic triblock copolymer $(PEO)_{106}(PPO)_{70}(PEO)_{106}$ (Pluronic F127, M_W = 12 600 provided by BASF), hydrochloric acid (HCl 35 wt %, from Prolabo), and absolute ethanol (EtOH, from Prolabo) were used as received. A synthetic procedure recently proposed to obtain PMOs by precipitation from the same reactants [10] was adapted to the aerosol technique. Typically, 0.9 g of F127 was added to 80 g of a mixture (50:50 wt %) of EtOH and 0.7 M HCl solution under mild stirring at room temperature. After complete dissolution, 3.22 g of BTEE was added. The mixture kept in a closed plastic bottle was stirred for 24 h under the same conditions before spray drying. The molar composition is the following: BTEE/F127/HCl/H_2O/EtOH = 1/0.00787/9/234/96.

Aerosol-generated spherical mesoporous particles were obtained by using the experimental setup shown in Fig. 2 [18]. The solution is poured into the atomizer; then a dry air flux (3 L min^{-1}) carries the resulting droplets, characterized by an initial mean diameter of 2 μm, into a furnace set at 673 K

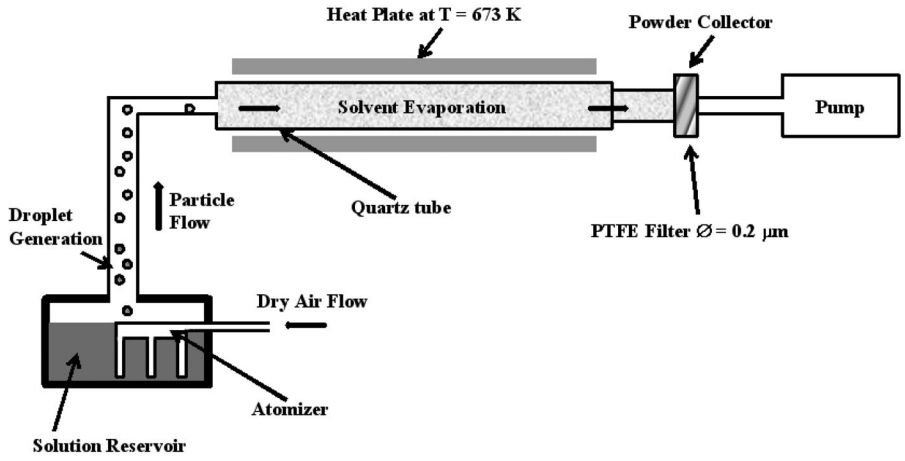

Fig. 2 Scheme of the aerosol generator apparatus.

(T amid the heated quartz tube $T \approx 473$ K) where evaporation occurs. The powders are then collected on a ($\varnothing = 0.2$ μm) PTFE filter (Biotech, Germany).

The as-synthesized particles are dried for at least 24 h at 323 K to further eliminate the residual solvent. The surfactant was removed according to the procedure reported by Guan et al. [21]: 1 g of as-synthesized particles is refluxed for 6 h at 323 K in 150 ml of absolute ethanol and 3.9 g of HCl 35 wt %. Conversion into SiCO glasses is achieved by pyrolysis under argon flow up to 1273 K for 2 h using a graphite crucible in a tubular furnace and a 5 K min^{-1} heating rate.

Characterization

The X-ray diffraction (XRD) patterns were recorded with a powder Bruker AXS D8 Advance Diffractometer in Bragg–Brentano configuration equipped with a graphite monochromator (Cu Kα radiation $\lambda = 0.154$ nm) in the range of $0.5° \leq 2\theta \leq 3°$.

Transmission electron microscopy (TEM) micrographs were recorded using a JEOL 100CXII electron microscope. Solid-state magic-angle spinning (MAS) NMR as well as cross-polarization coupled with MAS NMR (CP-MAS NMR) spectra were collected with a Bruker Avance 300 MHz spectrometer using a 4-mm Bruker probe spinning at 5 kHz. ^{29}Si and ^{13}C NMR experiments were carried out at frequencies of 59.62 and 75.47 MHz, respectively. For ^{29}Si MAS NMR analysis, 30° pulse (2.5 μs) and 60 s-recycle delay were used while ^{13}C CP-MAS NMR measurements were achieved with a contact time of 800 μs and a recycle delay of 2 s. Chemical shifts are referred to tetramethylsilane.

N_2 adsorption/desorption isotherms were measured at 77 K using a Micromeritics ASAP 2010 surface analyzer at a relative pressure of p/p_0 ranging from 0.05 to 0.99. Samples were outgassed overnight at 413 K before analysis. The specific surface area was determined by the Brunauer–Emmet–Teller (BET) method in the range of $0.05 \leq p/p_0 \leq 0.30$. The thermogravimetric analysis (TGA) was performed under argon flow using a NETZSCH STA 409 PC/PG analyzer (heating rate 5 K min^{-1} and Al_2O_3 crucible). Elemental analysis of the ceramic product was carried out by hot gas extraction.

RESULTS AND DISCUSSION

Characterization of surfactant-extracted PMO particles

Surfactant-extracted PMO particles were first characterized to verify their suitability as SiCO precursor. Scanning electron microscopy (SEM) pictures (not reported here) display spherical particles with a large distribution in size, between a few micrometers in diameter down to 20–30 nm. Powder XRD pattern of those particles shown in Fig. 3a reveals only one single broad peak at $2\theta \approx 0.85°$ (d-spacing = 10.4 nm), suggesting a worm-like structure of the pores. A comparison between this d-spacing value and the value associated with the most intense peak for the precipitated powders ($2\theta = 0.73°$, d-spacing = 12.6 nm, see Table 1) shows a shift to shorter distances, which can be related to a difference in the temperature process ($T \approx 473$ K for aerosol process and $T = 313$ K for precipitation), that produces extra shrinkage in the aerosol-generated powders.

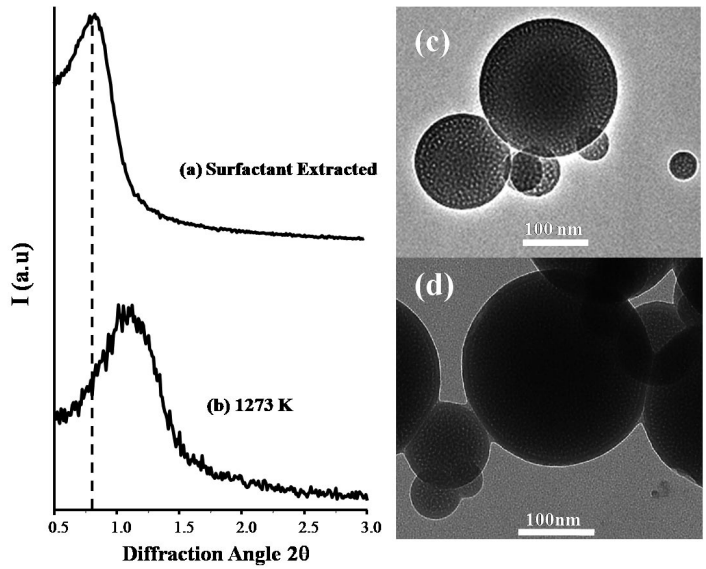

Fig. 3 XRD patterns of (a) PMO and (b) 1273 K pyrolysis product. TEM micrograph of (c) PMO and (d) 1273 K pyrolysis product.

Table 1 Comparison between nanoparticles prepared from precipitation and aerosol methods: XRD and N_2 adsorption/desorption data.

Synthetic method	Sample	d-Spacing/nm	V_{pore}/cm^3 g^{-1}	S_{BET}/m^2 g^{-1}
Precipitation	PMO	0.73	0.7	1075
	1273 K	0.95	0.2	262
Aerosol	PMO	0.85	0.12	144
	1273 K	1.10	–	16

The TEM micrograph (Fig. 3c) confirms the presence of spherical particles distributed in size. In agreement with the XRD pattern, the pores present a worm-like arrangement with average size of ≈6 nm, well within the size range for mesopores. Interestingly, a surface layer of about 10 nm surrounding the particles can be observed.

The corresponding N_2 adsorption/desorption isotherm is relatively close to a type IV isotherm (Fig. 4a), which is characteristic of mesoporous samples according to the IUPAC classification. However, this assumption has to be considered carefully since the isotherm exhibits an open hysteresis extended over the complete isotherm. The experiment was repeated several times to avoid experimental errors but the same behavior was always observed, and will be discussed later. The corresponding specific surface area can be estimated at 144 $m^2\ g^{-1}$ and the total pore volume and average pore diameter at 0.12 $cm^3\ g^{-1}$ and 3.3 nm, respectively (the latter value was calculated as $d = 4V/A$ where V is the total pore volume and A is the BET specific surface area).

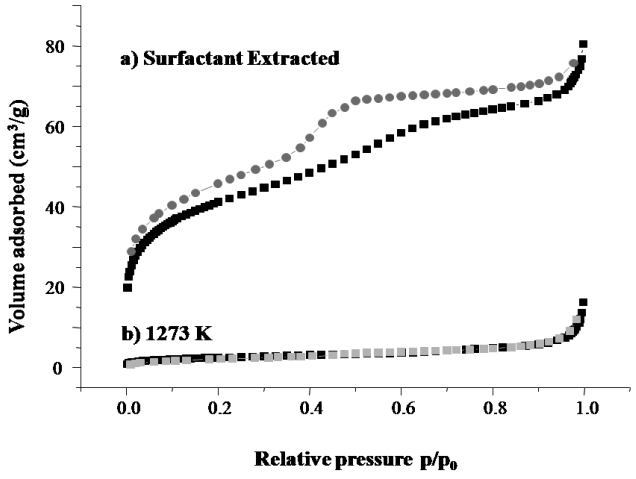

Fig. 4 N_2 adsorption/desorption isotherms of (a) PMO and (b) 1273 K pyrolysis product.

The chemical nature of the sample was investigated by ^{29}Si and ^{13}C solid-state NMR analysis. After solvent extraction, ^{29}Si MAS NMR spectrum (Fig. 5a) shows only one broad signal ranging from ≈ –40 to ≈ –70 ppm that corresponds to T^n units [C<u>Si</u>$(OX)_{3-n}(OSi)_n$] where X = H or CH_2CH_3. At least two T signals may be identified: the main one at –53 ppm (T^2 units [C<u>Si</u>$(OX)(OSi)_2$]) and the minor one at –60 ppm (T^3 units [C<u>Si</u>$(OSi)_3$]). Furthermore, the absence of any signal in the region between –80 and –110 ppm confirms that no Q^n units [<u>Si</u>$O_n(OX)_{n-4}$] were formed. All the Si–C bonds are thus preserved during the synthesis process resulting in a true organosilica framework. The simulation of the MAS NMR spectrum allows the identification and quantification of all T^n units with 51 % of T^2 units, 47 % of T^3 units and 2 % of T^1 units. The resulting framework is thus partially condensed.

The ^{13}C CP MAS NMR spectrum (Fig. 5c) reveals two main signals: the most intense at ≈5 ppm related to the ethane Si–<u>C</u>H_2–<u>C</u>H_2–Si linkages and a second one, corresponding to two overlapping components (at ≈71 ppm –O–<u>C</u>H_2– <u>C</u>H_2–O– and at ≈76 ppm –O–<u>C</u>H–(CH_3)–<u>C</u>H_2–O) related to incompletely extracted F127. The first signal is the most intense in agreement with the chemical formula of F127, $(PEO)_{106}(PPO)_{70}(PEO)_{106}$. The two signals at ≈18 and ≈60 ppm correspond to ethoxy groups (SiO–<u>C</u>H_2<u>C</u>H_3) grafted to the silica surface during the surfactant extraction procedure performed in refluxed ethanol. The peak at ≈18 ppm also contains a minor contribution due to the CH_3 groups from the PPO groups of F127.

PMO spherical porous particles have thus been generated via an aerosol-based procedure. However, they present limited N_2 adsorption ability leading to an uncommon loop shape and consequently a rather low surface area value (S_{BET} = 144 $m^2\ g^{-1}$), especially compared to the related precipitated powders (S_{BET} = 1075 $m^2\ g^{-1}$) or other aerosol-derived powders (generally $S_{BET} > 400\ m^2\ g^{-1}$ [18,22]). The loop can be explained by slow gas diffusion into the lesser accessible inner regions of the

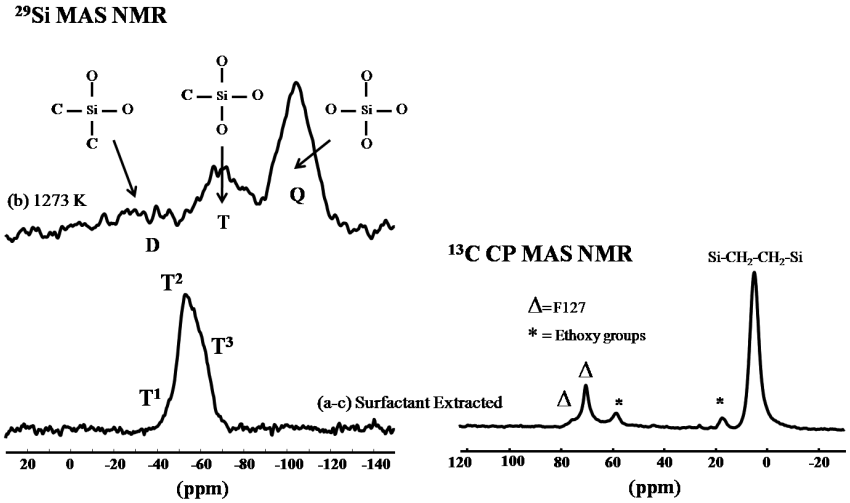

Fig. 5 ^{29}Si MAS NMR of (a) PMO and (b) 1273 K pyrolysis product. ^{13}C CP MAS NMR of (c) PMO.

particles [23]. This lack of accessibility could be due to incompletely removed surfactant (see ^{13}C NMR). However, in the precipitated sample in which F127 is also partially removed [10], a much higher S_{BET} is observed. Another hypothesis can be proposed based on the observation of a denser layer around the particles on the TEM micrographs. A literature survey shows that a similar phenomenon has already been observed and seems to be due to the specific use of F127 as structuring agent. For example, Baccile et al. [18] prepared mesoporous silica nanoparticles using either ionic or non-ionic surfactants. Only in the case of the Pluronic F127-structured sample, an outer layer is clearly visible by TEM, but unfortunately no data regarded the accessibility of the porosity are reported. The porous nanoparticles prepared with the other surfactants (CTAB, Brij-58, and P123) all exhibit quite high surface areas (S_{BET} > 540 m^2 g^{-1}) and microporous interconnectivity. Such an outer shell was also observed for mesoporous carbonaceous particles, obtained from a carbon precursor and Pluronic F127 [24]. In this case, the adsorption/desorption isotherm presents nearly an open hysteresis loop very similar to what we also observed.

These examples suggest that this particular behavior is due to the use of F127 as structuring agent. One may notice that F127 has the highest critical micelle concentration (cmc) with respect to the other commonly used templates, and is also the largest in size. This may affect the mobility of the species within the liquid droplets, leading to an enrichment of the surface with lighter siliceous species, and thus the formation of a denser silicon-rich outer layer. However, despite this low specific surface area, the particles were pyrolyzed to see whether they could be converted into a ceramic material with accessible porosity.

Characterization of SiCO glass particles

TGA (Fig. 6) was performed up to 1273 K under argon flow. A total weight loss of ≈30 % is observed. The initial weight loss (≈7 %) below 473 K comes from thermo-desorption of water and/or residual ethanol. Around 473 K, the residual F127 starts to decompose. Since pure F127 is supposed to be completely decomposed at 683 K [25], the second weight loss of ≈17 % that is observed up to 673 K, can be primarily related to surfactant decomposition. A third weight loss (≈6 %) up to 873 K may concern redistribution of Si–C and Si–O bonds in the network.

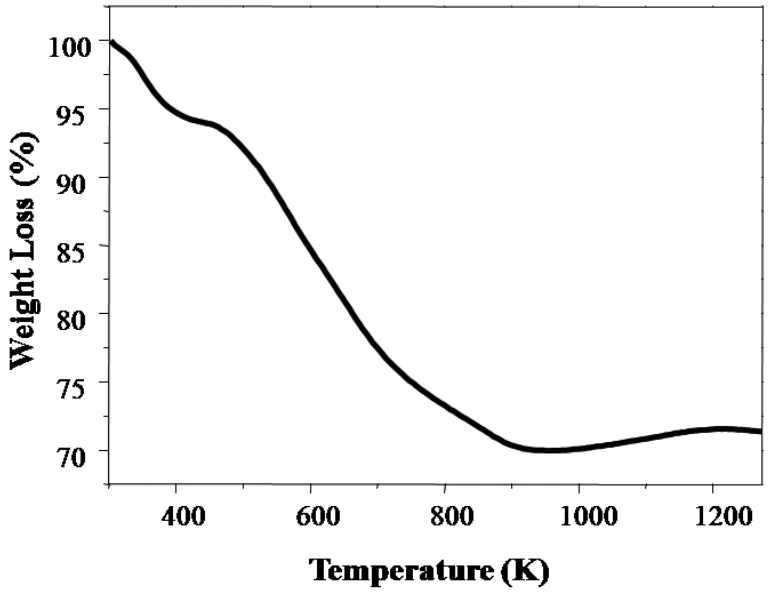

Fig. 6 TG curve recorded on PMO under argon flow.

After pyrolysis at 1273 K under argon flow, the whitish precursor turned black and the resulting powders were characterized to determine the chemical nature of the sample and to see whether any porosity has been retained after pyrolysis.

The XRD pattern (Fig. 3b) still displays a rather intense peak denoting that some ordering is still present after pyrolysis. The peak is slightly shifted toward higher angles ($2\theta \approx 1.10°$) and the *d*-spacing is reduced to 8.0 nm, which corresponds to a contraction of 23 %, the same value as the one observed for the precipitated powders. This is a consequence of structural rearrangement with simultaneous network and pore contraction. The TEM micrograph presented in Fig. 3d reveals that these particles have retained their spherical shape and still possess a worm-like network of mesopores. The ^{29}Si MAS NMR spectrum of the pyrolyzed sample (Fig. 5b) is characteristic of a true SiCO phase with signals corresponding to a distribution of SiC_xO_{4-x} units (where $0 \le x \le 4$). Ceramization modified both silicon and carbon local environment leading to a redistribution of the Si and C sites in the network. Indeed, at 1273 K three signals at –104, –70, and –30 ppm can be clearly identified as *Q* [$x = 0$; 56 %], *T* [$x = 1$; 30 %], and *D* [$x = 2$; 14 %] units, respectively. The presence of *Q* and *D* signals reveals that during pyrolysis, concomitant cleavage and formation of Si–C bonds occurred. Furthermore, the shift of the *T* signal to lower ppm values (–70 ppm instead of –60 ppm in the as-synthesized PMO) suggests a drastic change in the local environment of carbon atoms directly bonded to silicon, via the transformation of C–H bonds into C–Si bonds. ^{29}Si MAS NMR spectrum clearly demonstrates that a true SiCO phase is formed: assuming that at 1273 K, each C atom is bonded to 4 Si atoms, the spectrum simulation allows estimation of the stoichiometry for the SiCO phase: $SiC_{0.15}O_{1.71}$. This composition is quite similar to what has been found for the precipitated powders (see Table 2). Elemental analysis gives a C/Si molar ratio of 0.73, showing that the SiCO phase incorporates only 20 mol % of the total carbon, and that a free carbon phase has formed. Comparison between the ^{29}Si NMR data and elemental analysis leads to the following molar composition for the pyrolyzed SiCO glass particles: $SiC_{0.15}O_{1.71}$ + 0.58 C_{free}.

Table 2 ^{29}Si MAS NMR characterization of the SiCO phase in the pyrolysis product (1273 K) obtained via precipitation and aerosol methods.

Synthetic method	X and/or M (%) (δ/ppm)	D (%) (δ/ppm)	T (%) (δ/ppm)	Q (%) (δ/ppm)	SiCO phase ratio	C/Si molar
Precipitation	3 (–6)	13 (–35)	32 (–72)	52 (–105)	$Si\,C_{0.17}\,O_{1.66}$	0.62
Aerosol		14 (–30)	30 (–70)	56 (–104)	$Si\,C_{0.15}\,O_{1.71}$	0.73

While in the precipitated pyrolyzed powders, the isotherm is still of type IV and the specific surface area reduced to a significant value of 260 $m^2\ g^{-1}$, the aerosol-generated pyrolyzed particles are characterized by an isotherm typical for nonporous materials (Fig. 4b), which is confirmed by the very low S_{BET} value (16 $m^2\ g^{-1}$). Thus, despite the presence of mesopores revealed by the TEM micrograph, the outer layer has certainly totally densified, preventing gas from penetrating within the particles.

CONCLUSION

PMO submicrometric spherical particles have been prepared by an aerosol technique, starting from 1,2-bis(triethoxysilyl)ethane as organosilane and Pluronic F127 as structuring agent. The analysis by XRD and TEM reveals a worm-like arrangement of the pores with a specific surface area of 144 $m^2\ g^{-1}$. After pyrolysis under argon at 1273 K, ^{29}Si MAS NMR experiments and chemical analysis indicate that an oxycarbide network is obtained, together with the formation of a free carbon phase. The following composition can be deduced: $SiC_{0.15}O_{1.71} + 0.58\ C_{free}$. At 1273 K, the porosity is retained according to TEM micrograph, but the pores are not accessible most probably because of the densification of an outer surface layer that was already revealed in the starting PMO material. Work is currently in progress to increase the surface area of aerosol-generated PMO particles and retain the accessibility to this mesoporosity after pyrolysis.

ACKNOWLEDGMENTS

We thank the European Community who supported this work through the Marie Curie Research Training Network PolyCerNet (Contract MRTN-CT-2005-019601). We also thank the Feststoffe Fachbereich Material Laboratories at the Technical University of Darmstadt (Germany) for their kind assistance in elemental analysis.

REFERENCES

1. C. T. Kresge, M. E. Leonowicz, W. J. Roth, J. C. Vartuli, J. S. Beck. *Nature* **359**, 710 (1992).
2. S. Inagaki, S. Guan, Y. Fukushima, T. Ohsuna, O. Terasaki. *J. Am. Chem. Soc.* **121**, 9611(1999).
3. B. J. Melde, B. V. T. Holland, C. F. Blanford, A. Stein. *Chem. Mater.* **11**, 3302 (1999).
4. T. Asefa, M. J. MacLachlan, H. Grondey, N. Coombs, G. A. Ozin. *Angew. Chem., Int. Ed.* **39**, 1808 (2000).
5. F. Hoffmann, M. Cornelius, J. Morell, M. Fröba. *J. Nanosci. Nanotechnol.* **6**, 265 (2006).
6. (a) F. Hoffmann, M. Cornelius, J. Morell, M. Fröba. *Angew. Chem., Int. Ed.* **45**, 3216 (2006); (b) F. Hoffmann, M. Cornelius, J. Morell, M. Fröba. *Angew. Chem.* **118**, 3290 (2006).
7. B. Toury, R. Blum, V. Goletto, F. Babonneau. *J. Sol-Gel Sci. Technol*. **33**, 99 (2005).
8. B. Toury, F. Babonneau. *J. Eur. Ceram. Soc.* **25**, 265 (2005).
9. S. Masse, G. Laurent, F. Babonneau. *J. Non-Cryst. Solids* **353**, 1109 (2007).

10. A. Pauletti, S. Handjani, C. Fernandez-Martin, C. Gervais, F. Babonneau. *J. Ceram. Soc. Jpn.* **116**, 449 (2008).
11. G. D. Sorarù, E. Dalla Piccola, G. D'Andrea. *J. Am. Ceram. Soc.* **79**, 2074 (1996).
12. T. Rouxel, G. Massouras, G. D. Sorarù. *J. Sol-Gel Sci. Technol.* **14**, 83 (1999).
13. N. Keller, C. Pham-Huu, C. Crouzet, M. J. Ledoux, S. Savin-Poncet, J. B. Nougayrede, J. Bousquet. *Catal. Today* **53**, 535 (1999).
14. Y. Kim, S. R. Kim, K. H. Cho, S. Y. Bae, W. T. Kwon. *Ecomaterials Processing and Design*, p. 510, VII Trans Tech Publications, Zurich (2006).
15. C. J. Brinker, Y. Lu, A. Sellinger, H. Fan. *Adv. Mater.* **11**, 579 (1999).
16. C. Sanchez, C. Boissière, D. Grosso, C. Laberty, L. Nicole. *Chem. Mater.* **20**, 682 (2008).
17. Y. Lu, H. Fan, A. Stump, T. L. Ward, T. Rieker, C. J. Brinker. *Nature* **398**, 223 (1999).
18. N. Baccile, D. Grosso, C. Sanchez. *J. Mater. Chem.* **13**, 3011 (2003).
19. N. Baccile, A. Fischer, B. Julian-Lopez, D. Grosso, C. Sanchez. *J. Sol-Gel Sci. Technol.* **47**, 119 (2008).
20. C. Boissière, D. Grosso, H. Amenitsch, A. Gibaud, A. Coupé, N. Baccile, C. Sanchez. *Chem. Commun.* **22**, 2798 (2003).
21. S. Guan, S. Inagaki, T. Oshuna, O. Terasaki. *J. Am. Chem. Soc.* **122**, 5660 (2000).
22. X. Ji, Q. Hu, E. Hampsey, X. Qiu, L. Gao, J. He, Y. Lu. *Chem. Mater.* **18**, 2265 (2006).
23. F. Rouquerol, J. Rouquerol, K. Sing. *Adsorption by Powders and Porous Solids*, pp. 205, 297, Academic Press (1999).
24. Y. Yan, F. Zhang, Y. Meng, B. Tu, D. Zhao. *Chem. Commun.* **27**, 2867 (2007).
25. D. Long, F. Lu, R. Zhang, W. Qiao, L. Zhan, X. Liang, L. Ling. *Chem. Commun.* **14**, 2647 (2008).